

TiC: Exploring Vision Transformer in Convolution

Song Zhang^{*1} Qingzhong Wang^{*1}, Jiang Bian¹, Haoyi Xiong^{†1}

¹Baidu Inc.

Abstract

While models derived from Vision Transformers (ViTs) have been phonemically surging, pre-trained models cannot seamlessly adapt to arbitrary resolution images without altering the architecture and configuration, such as sampling the positional encoding, limiting their flexibility for various vision tasks. For instance, the Segment Anything Model (SAM) based on ViT-Huge requires all input images to be resized to 1024×1024. To overcome this limitation, we propose the Multi-Head Self-Attention Convolution (MSA-Conv) that incorporates Self-Attention within generalized convolutions, including standard, dilated, and depthwise ones. Enabling transformers to handle images of varying sizes without retraining or rescaling, the use of MSA-Conv further reduces computational costs compared to global attention in ViT, which grows costly as image size increases. Later, we present the Vision Transformer in Convolution (TiC) as a *proof of concept* for image classification with MSA-Conv, where two capacity enhancing strategies, namely Multi-Directional Cyclic Shifted Mechanism and Inter-Pooling Mechanism, have been proposed, through establishing long-distance connections between tokens and enlarging the effective receptive field. Extensive experiments have been carried out to validate the overall effectiveness of TiC. Additionally, ablation studies confirm the performance improvement made by MSA-Conv and the two capacity enhancing strategies separately. Note that our proposal aims at studying an alternative to the global attention used in ViT, while MSA-Conv meets our goal by making TiC comparable to state-of-the-art on ImageNet-1K. Code will be released at <https://github.com/zs670980918/MSA-Conv>.

Introduction

Images have become indispensable to our daily life, leading to massive image data generation and collection to enable ubiquitous applications in various domain (Guo et al. 2022). Vision transformer (ViT) architectures (Dosovitskiy et al. 2020) have emerged as one of the most promising ways to handle vast image data (Bommasani et al. 2021) for versatile pattern recognition (Theodoridis and Koutroumbas 2006) and image understanding tasks (Weems et al. 1989). For instance, Segment Anything Model (SAM) (Kirillov et al. 2023) with more than 100M learnable parame-

ters, pre-trained on large-scale general-purpose instance segmentation and scene parsing datasets such as COCO (Lin et al. 2014) and ADE20K (Zhou et al. 2017), could perform zero-shot segmentation on images from various data sources without further tuning.

Specifically, in the ViT design, images are segmented into discrete non-overlapping patches, typically sized at 16 × 16 (Fan et al. 2021). These patches are then treated as tokens, analogous to the tokens in NLP tasks (Wu et al. 2021), and integrated with positional encoding to represent coarse-grained spatial information. Subsequently, the data undergoes repeated standard transformer layers to model global relations (Dosovitskiy et al. 2020), ultimately enabling effective image classification.

While ViT-based models have achieved remarkable success in various vision tasks, they might not be able to be applied to high-resolution images without changing the architecture or configuration like re-sampling the positional encoding (Li et al. 2022), limiting the accessibility of models to various vision tasks. For instance, SAM based on ViT-Huge requires all input images to be resized to 1024×1024. In contrast, convolutional architectures like ResNet (He et al. 2016) are able to handle images of arbitrary resolutions. Furthermore, as the scale of input images increases, ViT-based models with global attention incur substantial computational overhead, hindering their ability to handle high-resolution images (Liu et al. 2021).

To overcome these limitations and unlock the full potential of ViT for high-resolution images, we propose a novel approach that enhances the adaptability and computational efficiency of ViT. Our proposed Multi-Head Self-Attention Convolution (MSA-Conv) mechanism allows ViT to accept images with arbitrary resolution, eliminating the requirement of resizing or re-sampling the positional encoding, and facilitating seamless integration into various vision tasks. MSA-Conv leverages the power of convolutions, such as standard convolution (Bouvier 2006), dilated convolution (Yu and Koltun 2015), and depthwise convolution (Chollet 2017), which can be applied to arbitrary image resolution.

Further, during our exploration of constructing novel architectures with MSA-Conv, we observe that replacing global attention used in ViT with MSA-Conv would result in sub-optimal performance on the ImageNet-1K (Deng et al. 2009) image classification task. Such degradation, however,

^{*}These authors contributed equally.

[†]Corresponding author

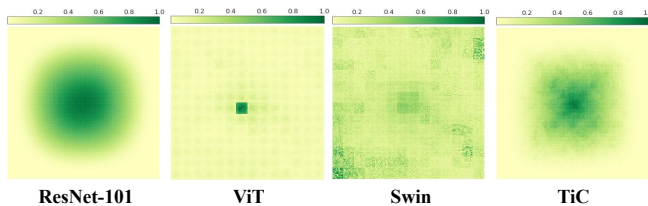


Figure 1: Effective receptive field (Luo et al. 2016b) of the mainstream backbones and TiC.

can be mitigated with the adoption of larger kernel sizes in MSA-Conv. This observation inspires us to study the effective receptive field problem, as MSA-Conv simply combining convolution with self-attention (Vaswani et al. 2017b) would cause similar kernel size issues in convolutional neural networks (Luo et al. 2016b). Hereby, in this paper, we present Vision Transformer in Convolution (TiC)—a proof-of-concept ViT design incorporating our proposed MSA-Conv with two advanced strategies as follows.

- *Multi-Directional Cyclic Shifted Mechanism*: Inspired by Swin (Liu et al. 2021), TiC adopts a token shift mechanism to establish long-distance connections, employing four distinct manners to establish connections between diagonal position tokens for long-range connectivity.
- *Inter-Pooling Mechanism*: To avoid the additional computational overhead caused by the use of larger kernel sizes, TiC adopts an inter-pooling mechanism to reduce the size of the token map while enlarging the effective receptive field by pooling neighboring tokens.

Above two strategies, together with patch downsample layers in TiC, could efficiently enlarge the effective receptive field and improve performance substantially, without significantly consuming computational costs. To understand the effectiveness of MSA-Conv and TiC over existing architectures, we visualize and compare the effective receptive fields obtained by four architectures, including ResNet-101, ViT, Swin and TiC. Figure 1 illustrates the effective receptive fields of the four architectures on the same image. The effective receptive field of our newly proposed TiC demonstrates a resemblance to ResNet-101 (He et al. 2016), which gives precedence to pixels near the center by assigning them larger weights. In contrast, ViT leans towards assigning maximum weight to the exact center, while the Swin shows a tendency to attribute greater importance to pixels distanced from the center. The observation back-ups the motivation of our proposal that incorporates convolution within transformers.

Comprehensive experimental evaluations have been conducted to ascertain the overarching efficacy of MVS-Conv. Furthermore, through ablation analyses, the enhancements introduced by MSA-Conv and the two capacity enhancing strategies have been individually validated. It is important to emphasize that our endeavor revolves around investigating an alternative to the global attention mechanism employed in ViT. MSA-Conv aligns with our objectives by rendering TiC competitive with state-of-the-art benchmarks on the ImageNet-1K dataset. Note that, though MSA-Conv and TiC are part of contributions claimed in this work, they might not be the best solutions in many of our experiments. However,

both ablation studies and overall evaluation have proved the concepts of incorporating convolution within transformers with MSA-Conv, enlarging effective receptive fields via two strategies, and allowing images of arbitrary resolutions in TiC. Additional efforts are requested along this line of research for providing product-grade solutions.

Related Work

Convolutional-Based models have been at the forefront of computer vision for several decades (Krizhevsky, Sutskever, and Hinton 2012; Simonyan and Zisserman 2014; Szegedy et al. 2015). The seminal work of AlexNet (Krizhevsky, Sutskever, and Hinton 2012) catapulted CNNs into the mainstream, leading to the development of deeper and more effective Conv-Based architectures, including VGG (Simonyan and Zisserman 2014), GoogleNet (Szegedy et al. 2015), ResNet (He et al. 2016), DenseNet (Iandola et al. 2014), HRNet (Wang et al. 2020), and EfficientNet (Tan and Le 2019). Furthermore, research efforts have been devoted to enhancing individual convolution layers, resulting in innovations such as depthwise convolution (Chollet 2017) and deformable convolution (Dai et al. 2017).

In recent years, ViT models have garnered increasing attention and demonstrated significant success in computer vision tasks (Han et al. 2022). Pioneering work like ViT (Dosovitskiy et al. 2020) directly applied the transformer architecture from NLP to image classification using image patches as input. Subsequent studies, such as Swin (Liu et al. 2021) and CSWin (Dong et al. 2022), have further explored self-attention within shifted local windows, and PVT (Wang et al. 2021) introduced a pyramid structure to generate multi-scale feature maps for pixel-level dense prediction tasks. Moreover, CPVT (Chu et al. 2021) and CvT (Wu et al. 2021) leveraged a convolutional projection into transformers.

However, current pre-trained models (He et al. 2022; Xie et al. 2022) cannot directly apply to high-resolution images without changing the architecture and configuration like resampling the positional encoding (Li et al. 2022), limiting the flexibility compared to Conv-Based architectures. To capitalize on the strengths of both approaches, we draw inspiration from the sliding window mechanism of convolution and integrate it into the ViT-based models. This fusion aims to enhance performance and flexibility in computer vision applications, leveraging the advantages of Conv-Based architectures and ViTs simultaneously.

Methodology

While the major claim of this work is the proposal of Multi-head Self-Attention Convolution (MSA-Conv), as an alternative to the global attention used in ViT. We also introduce Vision Transformer in Convolution (TiC) as a *proof of concept* solution leveraging MSA-Conv for image classification of arbitrary resolutions. Here, we first present the overall design of TiC, then specify the design of MSA-Conv in details.

Framework

Overall Design of TiC As shown in Figure 2, TiC adopts a hierarchical architecture consisting of several MSA-Conv

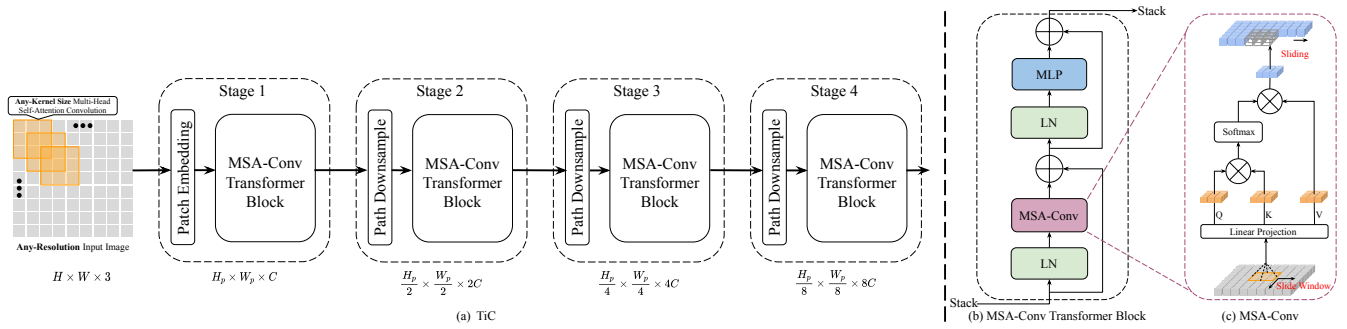


Figure 2: (a) The architecture of TiC; (b) the architecture of MAS-Conv Transformer Block; (c) the illustration of MSA-Conv.

Transformer Blocks and Patch Downsample layers, where every block leverages an any-kernel size multi-head self-attention convolution facilitating feature extraction and learning from images of diverse resolutions in a transformer layer. Specifically, in “Stage 1” of TiC, the initial MSA-Conv Transformer Block processes the token features from the patch embedding module, preserving the full spatial resolution of $H \times W$ tokens. To introduce a hierarchical representation, the patch downsample layer progressively reduces the number of tokens as the network depth increases. Specifically, the first downsample layer concatenates the features of each 2×2 neighboring patch group, resulting in $4C$ -dimensional features. These features are then projected by a linear layer to $2C$ dimensions, effectively reducing the number of tokens by a factor of 4 ($2 \times$ downsampling of spatial resolution). Subsequent MSA-Conv Transformer Blocks operate on this lower resolution feature map of $H_p \times W_p$ ($H_p = \frac{H}{4}$, $W_p = \frac{W}{4}$), constituting “Stage 2” of TiC. To the end, such hierarchical design effectively combines multi-scale feature learning with long-range modeling.

MSA-Conv Transformer Block More specifically, inside every MSA-Conv Transformer Block, the standard multi-head self-attention (MSA) module used by the vanilla Transformer block is replaced by an any-kernel size multi-head self-attention convolution (MSA-Conv), while the remaining layers remain unchanged. As depicted in Figure 2, an MSA-Conv Transformer Block consists of the MSA-Conv module, followed by a 2-layer MLP (Tolstikhin et al. 2021) with GELU (Hendrycks and Gimpel 2016) nonlinearity in between. LayerNorm (LN) (Ba, Kiros, and Hinton 2016) layers are applied before each MSA-Conv module and each MLP, with a residual connection applied after each module.

Feature Extraction and Outputs The process involving MSA-Conv Transformer Blocks and Patch Downsample layers is repeated twice more, constituting “Stage 3” and “Stage 4”, which yield feature maps at spatial resolutions of $\frac{H}{16} \times \frac{W}{16}$ and $\frac{H}{32} \times \frac{W}{32}$, respectively. This hierarchical architecture allows the network to generate a multi-scale feature representation, comparable to resolutions typically produced by convolutional backbones such as VGG (Simonyan and Zisserman 2014) and ResNet (He et al. 2016). As a result, the proposed architecture can easily replace backbone networks in existing methods for various computer vision tasks.

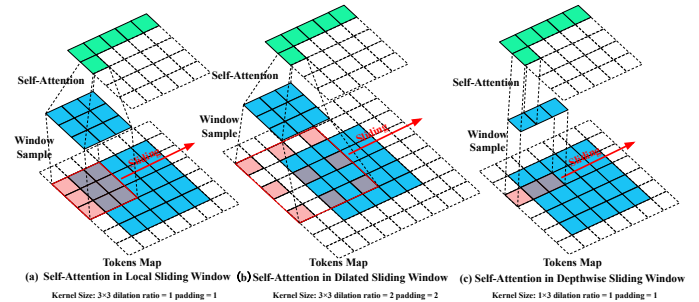


Figure 3: Illustration of MSA-Conv operations. (a): the self-attention w/. local sliding window; (b): w/. dilated sliding window; (c): w/. depthwise sliding window.

Multi-Head Self-Attention Convolution

The Vision Transformer architecture (Dosovitskiy et al. 2020) and its adaptation for image classification employ global self-attention, where the relationships between a token and all other tokens are computed. However, the global computation leads to quadratic complexity concerning the number of tokens, rendering it unsuitable for many vision tasks that require an extensive set of tokens for dense prediction or to represent high-resolution images. To address this limitation, the Swin-Transformer (Liu et al. 2021) proposes local self-attention, wherein self-attention is computed within local windows, reducing computational demand. While these methods demonstrate excellent performance in image classification, they process different resolutions images need to re-sample the positional encoding (ViT (Dosovitskiy et al. 2020)) or adjust the configuration of architecture (Swin-Transformer (Liu et al. 2021)).

To address these challenges and enable the flexible processing of any-resolution input images while fully utilizing local attention within an any-kernel size window, we introduce the Multi-Head Self-Attention Convolution (MSA-Conv). This mechanism allows for self-attention computation within a local sliding window of any kernel size, akin to the convolutional mechanism. We have implemented MSA-Conv as a convolutional layer, which further enhances its ease of integration within various vision architectures.

Self-Attention in Local Sliding Window Local attention has demonstrated its effectiveness in the Swin-Transformer (Liu et al. 2021) architecture. In our proposed attention pattern, we employ a combination of fixed-size window atten-

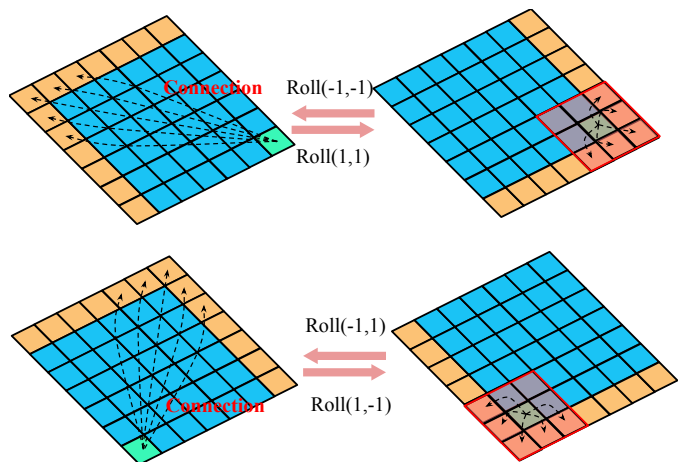
tion surrounding each token and flexible-size window attention across different layers. The use of multiple stacked layers of such window attention enables a large receptive field, granting top layers access to all input locations and the capacity to build representations incorporating information across the entire input, akin to CNNs (Luo et al. 2016a). The local sliding window illustration is provided in Fig. 3(a). Let us assume that each window contains $M \times M$ patches in a layer, and the kernel size of MSA-Conv is $K \times K$. The computational complexity of a local sliding window-based MSA on an image with $h \times w$ patches is depicted as follows in Eq. (1) $\Omega(\text{MSA} - \text{Conv})$:

$$\begin{aligned} \text{TiC: } \Omega(\text{MSA} - \text{Conv}) &= 4hwC^2 + K^2hwC \\ \text{ViT: } \Omega(\text{MSA}) &= 4hwC^2 + 2(hw)^2C, \\ \text{Swin-T: } \Omega(\text{W} - \text{MSA}) &= 4hwC^2 + 2M^2hwC \end{aligned} \quad (1)$$

Furthermore, we have conducted a comparative analysis of computational complexity with ViT (Dosovitskiy et al. 2020) and Swin-Transformer (Swin-T) (Liu et al. 2021) in Eq. (1). As observed, the global self-attention computation ($\Omega(\text{MSA})$) generally becomes impractical for large hw dimensions, whereas the window-based self-attention ($\Omega(\text{MSA} - \text{Conv}), \Omega(\text{W} - \text{MSA})$) exhibits scalability. Both TiC and Swin-T demonstrate similar computational complexity, benefiting from the sliding window mechanism. Additionally, our MSA-Conv introduces the advantage of supporting any-resolution input images compared to other methods while maintaining similar efficiency.

Self-Attention in Dilated Sliding Window We aim for our MSA-Conv to function as a comprehensive convolutional layer, encompassing both the normal sliding window capability and a widely used dilated capability to enhance the receptive field of the local window. To achieve a broader receptive field without increasing computational overhead, we introduce the concept of "dilation" to the sliding window. This concept draws parallels with dilated CNNs (Yu and Koltun 2015), where gaps of size dilation d are introduced within the window. Assuming a fixed d and w for all layers, the resulting receptive field becomes $d \times h \times w$, potentially reaching hundreds of patch tokens even for small dilation values. In the context of multi-head self-attention, each self-attention head computes distinct attention scores. Inspired by this, we implement different dilation configurations per head to improve performance. This allows some heads without dilation to focus on local context, while others with dilation focus on the larger context. The illustration of the dilated sliding window is depicted in Fig. 3(b).

Self-Attention in Depthwise Sliding Window Figure 3(c) illustrates the mechanism of our depthwise sliding window. Based on this mechanism, our MSA-Conv can accommodate any-kernel size window (e.g., $1 \times K, K \times 1, K \times K$) for self-attention computation. Consequently, to increase the effective receptive field without significantly escalating computation, larger kernel sizes can be adopted to enhance performance. This concept shares similarities with depthwise CNNs (Chollet 2017), where each input channel



Multi-Directional Cyclic Shifted Mechanism

Figure 4: Illustration of overall Multi-Directional Cyclic Shifted Mechanism. Roll refers to (Paszke et al. 2019).

is convolved with a distinct kernel. Assuming the MSA-Conv possesses four self-attention heads, different kernel sizes can be employed for each self-attention head. In line with the above different dilation configurations per head, we also select one head to utilize a larger kernel size, resulting in a larger receptive field for focusing on the broader context.

Effective Receptive Field Enlargement Strategies

The local sliding window-based MSA-Conv module lacks connections among patch tokens in remote locations, limiting its modeling power. While the dilated sliding window and depthwise sliding window have enhanced the receptive field to some extent, they are not potent enough to establish connections between diagonal position tokens, essential for obtaining global task-specific representations. To address this limitation, we have devised strategies to establish long-distance connections, thereby enhancing the capability of task-specific information perception in our model.

Multi-Directional Cyclic Shifted Mechanism The local sliding window-based self-attention module lacks the capability of establishing long-distance connections across patch tokens, leading to limitations in its modeling power. Taking inspiration from Swin-Transformer (Liu et al. 2021), we propose a multi-directional cyclic shifted mechanism to introduce cross-token connections without incurring additional computation. This mechanism randomly cyclically shifts in four directions, enabling patch tokens that are difficult to relate due to the window size to be included in the same window. As a result, the receptive field is increased, thereby enhancing the capability of task-specific information perception in our model. The illustration of this mechanism is provided in Fig. 4. In our experiments, we ensure full interaction of information by setting the size of cyclic shifted to half of the window size, guaranteeing that a portion of the patch tokens originates from long-distance connections.

Inter-Pooling Mechanism To increase the receptive field for capturing more contextual information while simultane-

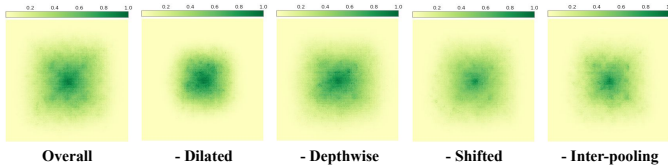


Figure 5: Illustration of the Impact of Different Modules on the Effective Receptive Field.

ously reducing computational complexity, we introduce an inter-pooling mechanism. This mechanism employs convolutions to pool the patch tokens, enabling the aggregation of additional neighboring context information within a single window. The formulation of our inter-pooling mechanism is defined as follows in Eq. 2:

$$\begin{aligned}
 \mathbf{Q}: & \text{Rerange}(\mathbf{Q}, f) \\
 \mathbf{K}: & \text{Repeat}(\mathbf{K} \odot w_1, \mathbf{Q}.shape) \\
 \mathbf{V}: & \text{Repeat}(\mathbf{V} \odot w_2, \mathbf{Q}.shape)
 \end{aligned} \tag{2}$$

where f represents pooling factor, \odot represents the Hadamard multiplication, w_i represents the weights of the convolutional layers. Specifically, for the query (\mathbf{Q}), we employ the Rerange operation (from the einops library (Rogozhnikov 2022)) to reshape \mathbf{Q} . The shape transformation formulation is as follows: $[B, C, H, W] \rightarrow [B \times f^2, C, \frac{H}{f}, \frac{H}{f}]$. As for the key (\mathbf{K}) and value (\mathbf{V}), we utilize separate convolutions to downsample (aggregate information) each item (shape: $[B, C, H, W] \rightarrow [B, C, \frac{H}{f}, \frac{H}{f}]$), and then adopt the Repeat operation (from the einops library (Rogozhnikov 2022)) to reshape the shape. The shape transformation formulation is: $[B, C, \frac{H}{f}, \frac{H}{f}] \rightarrow [B \times f^2, C, \frac{H}{f}, \frac{H}{f}]$. Through inter-pooling, we can efficiently aggregate information while simultaneously increasing the batch size for CUDA, achieving computational acceleration.

Experiments

In this section, we discuss the enhancement of model performance by effective receptive fields and perform related ablation experiments. And we also present an efficiency analysis of the proposed TiC architecture against previous state-of-the-art methods to validate the flexibility of our proposed MSA-Conv. Additionally, we conduct extensive experiments on ImageNet-1K image classification (Deng et al. 2009) to validate the effectiveness of our MSA-Conv based on TiC.

Effectiveness on Receptive Field Enlargement

In this section, we discuss the impact of the improvement of the receptive field brought about by different strategies on performance. Specifically, we conducted experiments based on ImageNet-1K image classification (Deng et al. 2009). The ablation study of each module is reported in Table 1. And the effective receptive field of each module is shown in Figure. 5.

Dilated Sliding Window As illustrated in Figure 5, it is evident that the removal of the dilated sliding window leads to a reduction in the effective receptive field of the model

	Backbone	ImageNet Top-1 acc (%)	ImageNet Top-5 acc (%)
- dilated	TiC-B	76.47	92.37
overall	TiC-B	79.00	94.31
- depthwise	TiC-B	78.72	94.22
overall	TiC-B	79.00	94.31
- cyclic shifted	TiC-B	78.46	93.78
overall	TiC-B	79.00	94.31
- inter-pooling	TiC-B	77.32	93.30
overall	TiC-B	79.00	94.31

Table 1: Ablation study on ImageNet-1K. '-' represents removing the module from the overall TiC.

compared to the overall TiC architecture (Figure 5 TiC vs. Figure 5 -Dilated). Furthermore, the implications of dilated sliding window ablations on classification performance are detailed in Table 1. Notably, TiC incorporating the dilated sliding window surpasses its local sliding window counterpart by a margin of 2.53 in terms of top-1 accuracy on the ImageNet-1K. These results substantiate the efficacy of leveraging the dilated sliding window to amplify the effective receptive field and foster connections between patch tokens spanning longer distances.

Depthwise Sliding Window As depicted in Figure 5, the utilization of the depthwise sliding window results in a discernible augmentation of the effective receptive field. Although the expansion of the effective receptive field through the depthwise sliding window is comparatively smaller when contrasted with the effects of the dilated sliding window, we posit that this discrepancy could be attributed to the application of the depthwise sliding window solely on a single head within the Multi-Head configuration. This observation is further substantiated through quantitative assessment, as highlighted in Table 1. Notably, TiC incorporating the depthwise sliding window achieves an increment of 0.28 in top-1 accuracy on the ImageNet-1K dataset when compared to its local sliding window counterpart. These outcomes underscore the efficacy of leveraging the depthwise sliding window to amplify the perceptual field and facilitate the establishment of connections between patch tokens spanning longer distances.

Multi-Directional Cyclic Shifted Mechanism As illustrated in Figure 5, our qualitative results reveal that the incorporation of the shifted mechanism generates a discernible elevation in attention towards edge tokens. This shift is perceptible through the darker coloration and extended range of the effective receptive field's edge, consequently fostering the establishment of connections between tokens situated at distant positions. This augmentation is anticipated to yield an enhancement in model performance. This empirical observation is corroborated by the quantitative outcomes, as detailed in Table 1. Specifically, our findings substantiate the efficacy of amplifying attention towards edge tokens in bolstering model performance. Notably, TiC integrating the multi-directional cyclic shifted mechanism exhibits a notable superiority over its counterpart devoid of this mechanism, showcasing a commendable increment of 0.54 in top-1 accuracy on the ImageNet-1K dataset.

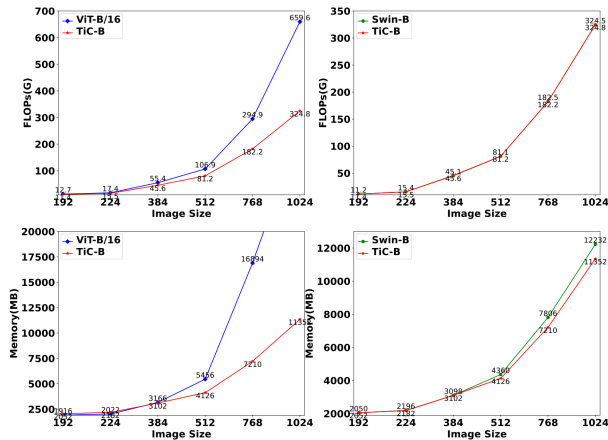


Figure 6: Efficiency Analysis. Comparative evaluation of FLOPs and memory usage between TiC and mainstream ViT-based models across various image resolutions in the inference phase.

Inter-Pooling Mechanism As depicted in Figure 5, a discernible enhancement in the effective receptive field is evident the implementation of inter-pooling. This augmentation is attributed to the aggregation of neighboring tokens within the same local window for self-attention. The consequence is an increase in the participation of tokens within self-attention, consequently fostering an expansion of the effective receptive field. The efficacy of our inter-pooling strategy is further substantiated by quantitative results. Quantitatively, the results demonstrate the superiority of TiC integrated with the inter-pooling mechanism over its counterpart lacking this mechanism. Specifically, TiC endowed with the inter-pooling mechanism showcases a noteworthy advancement of 1.68 in top-1 accuracy on the ImageNet-1K dataset. This numerical validation underscores the potency of the inter-pooling mechanism in enlarging the receptive field and thereby enhancing model performance.

In summary, drawn from the comprehensive ablation study analysis, it is evident that the effective receptive field plays a pivotal role in model performance. Therefore, enhancing the effective receptive field stands as a pivotal avenue for improving model performance in future endeavors.

Efficiency under Varying Image Resolutions

In this section, in order to further verify the flexibility and effectiveness of MSA-Conv on arbitrary resolution images, we compared the efficiency of various ViT-based models corresponding to different resolutions on ImageNet-1k in the inference phase. Moreover, we also discuss the runtime and memory of different implementations of TiC’s MSA-Conv in the inference phase.

Significantly, during our experimentation phase, a notable observation arose concerning the adaptability of ViT-B/16 and Swin-B to varying image resolutions. In the specific context of ViT-B/16 trained on images with dimensions of 224×224 , conducting inference on images of dissimilar res-

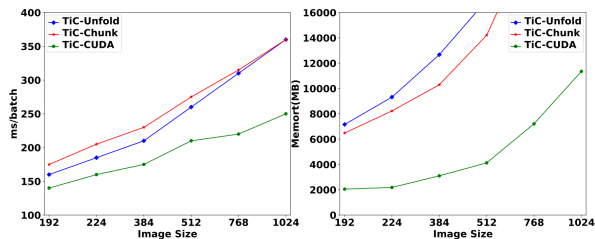


Figure 7: Illustration of efficiency analysis of different implementations of MSA-Conv in the inference phase.

olutions necessitates the resampling of positional encoding to ensure proper utilization. Similarly, Swin-B encounters limitations related to the interplay between window size and image size. For instance, for an image of size 224×224 , Swin-B mandates a window size adjustment to 7, while for an image of dimensions 192×192 , the optimal window size becomes 6. This inflexibility in adaptability is a discernible drawback in these architectures. In contrast, our MSA-Conv architecture leverages the advantages of sliding window mechanisms and potential positional encoding, endowing it with the capability to seamlessly function across diverse image resolutions without necessitating any modifications.

As shown in Figure 6, we can observe that our approach exhibits a distinct advantage over ViT with global attention in terms of FLOPs as image resolutions escalate. This observation is in alignment with the theoretical computational formulation described in Eq. (1). Notably, as the image dimensions reach 1024×1024 , the FLOPs of ViT-B/16 surge to almost twice that of TiC. This discrepancy underscores TiC’s computational efficiency in contrast to ViT-B/16. Furthermore, the escalating memory usage of ViT-B/16 due to its global attention computational mechanism is of paramount significance. The involvement of an increasing number of patch tokens in computation, which is exponentiated by the expanding image size, amplifies the memory usage in ViT-B/16. Conversely, our method capitalizes on the local sliding window mechanism for self-attention computation. Consequently, the memory usage of TiC grows linearly in relation to the image size, offering a more favorable trade-off between memory utilization and image dimensions. Comparison with Swin-B, which is also based on local attention, showcases a parallel performance in terms of FLOPs, a correspondence that aligns with the predictions posited by Eq. (1). Furthermore, leveraging the benefits of CUDA programming’s resource scheduling capabilities, as the image scale keeps increasing TiC will gradually be lower than Swin-B in terms of memory consumption, e.g., 1024×1024 , TiC: 11352MB vs. Swin-B 12232MB.

In addition, we conducted comparisons involving time and memory utilization across different implementations of TiC’s MSA-Conv. Our TiC implementation encompasses three variants: 1. TiC-Unfold, 2. TiC-Chunk, and 3. TiC-CUDA. TiC-Unfold employs the nn.Unfold interface (Paszke et al. 2019) from PyTorch to mimic a sliding window for value extraction, followed by self-attention computations using pure Python code. TiC-Chunk, an en-

Methods	Image size	FLOPs (G)	ImageNet Top-1 acc (%)	ImageNet Top-5 acc (%)
ViT-B/16	224 ²	55.4G	76.45	93.08
Swin-B	224 ²	15.4G	80.48	95.21
TiC-B	224 ²	15.5G	79.00	94.31

Table 2: Comparison of different backbones from scratch training on ImageNet-1K for classification. Throughput is measured using the GitHub repository of (Wightman 2019) and 8x V100-16G GPU, following (Touvron et al. 2021).

hancement of TiC-Unfold, processes values from nn.Unfold in batches to optimize memory consumption through pure Python code. TiC-CUDA relies on CUDA programming (Sanders and Kandrot 2010), utilizing C++ to implement underlying convolution calculation for forward and backward propagation, and leveraging CUDA for computational acceleration. In Figure 7, it is evident that our TiC-CUDA leverages CUDA’s computational advantages, surpassing the processing speed of both TiC-Unfold and TiC-Chunk. Furthermore, TiC-CUDA remarkably reduces memory consumption compared to its counterparts through matrix operations optimized via CUDA programming. CUDA’s inherent memory management capabilities further enhance the efficiency of our TiC-CUDA for processing tasks.

In summary, grounded in the comprehensive experimental analysis presented above, our assertion is that MSA-Conv exhibits heightened flexibility and efficiency in accommodating images of any-resolutions when juxtaposed with prevailing mainstream ViT-based models.

Effectiveness on Downstream Tasks

To validate the effectiveness of our MSA-Conv, we evaluate the TiC framework on the ImageNet-1K image classification (Deng et al. 2009). Our performance metric is the top-1 accuracy derived from a single crop. In the experimental setting, we use similar configurations as Swin-Transformer (Liu et al. 2021).

Results with ImageNet-1K from scratch training Table 2 showcases performance comparisons of our TiC-B architecture against prevalent Transformer-based backbones. These evaluations are carried out through ImageNet-1K training from scratch within our environment. In contrast to established state-of-the-art Transformer-based models, specifically ViT-B/16 and Swin-B, our TiC-B demonstrates a substantial enhancement in top-1 accuracy on ImageNet-1K, surpassing ViT-B by 2.55 and yielding a comparable outcome of 79 against Swin-B’s 80.48.

Results with ImageNet-1K pre-training and fine-tuning

We further perform pretraining of our TiC on the ImageNet1K dataset. Fine-tuned outcomes for ImageNet-1K image classification are presented in Table 3. When juxtaposed with prevailing state-of-the-art Transformer-based architectures, such as ViT-B/16 (81.79) and Swin-B (83.31), our TiC-B has achieved a commendably competitive top-1 accuracy of 80.71 on the ImageNet-1K benchmark. These findings suggest that there remains ample potential for further enhancements in our model’s performance.

Methods	Image size	ImageNet Top-1 acc (%)	ImageNet Top-5 acc (%)
ViT-B/16	224 ²	81.79	95.75
Swin-B	224 ²	83.31	96.36
TiC-B	224 ²	80.71	95.07

Table 3: Comparison of different backbones pretraining on ImageNet-1K and finetuning on ImageNet-1K. For the sake of fairness, we maintain uniformity in our experimental environment and configuration.

In summation, drawn from the outcomes of the above experiments, it is evident that MSA-Conv demonstrates performance on par with existing approaches in downstream image classification. Moreover, its substantial potential as versatile and overarching ViT-based models for future applications is notably discernible.

Discussion

Despite matching state-of-the-art-methods on ImageNet-1K tasks (Deng et al. 2009), our model reveals areas for improvement as follows.

- **Efficiency:** the C++/CUDA implementation of MSA-Conv presents inefficiencies because of computational overheads from intermediate value generation during **Dot** propagation stages. This may be mitigated by single-process computation of **Q**, **K**, **V** gradients, based on the backward gradient $\tilde{\mathbf{O}}$.
- **Extensibility:** Our previous section outlined MSA-Conv implementations in standard, dilated, and depthwise configurations. We suspect there would be an opportunity for MSA-Conv to include deformable convolution. This extension might allow self-attention to autonomously choose computational patches, leading to prospective enhancements in model performance. Additionally, considering implementation methods and effective receptive field boundaries, there seems to be potential for modular MSA-Conv within CNNs.

Thus, we advocate for future research in above areas.

Conclusion

This study presents a transformative proposal, MSA-Conv, that incorporates Self-Attention within generalized convolutions. This approach offers adaptability to Vision Transformers (ViTs) for handling images of variable resolutions without the need for retraining or rescaling, effectively addressing limitations faced in past ViT-based models like SAM. The introduction of Vision Transformer in Convolution (TiC) served as a proof of concept, demonstrating the pivotal role played by MSA-Conv, alongside two capacity enhancing strategies, in boosting the overall effectiveness of TiC. The efficacy of TiC was substantiated through several extensive experiments and ablation studies. This pursuit of finding a viable alternative to the global attention used in ViT found success in MSA-Conv, making TiC a comparable baseline against leading benchmarks on ImageNet-1K. Though TiC might not be the best solution in experimental

comparisons, however it sheds light on the future research directions of incorporating transformers in convolution, enlarging effective receptive fields for enhanced capacity, and handling images of arbitrary/variable resolutions.

References

- Ba, J. L.; Kiros, J. R.; and Hinton, G. E. 2016. Layer normalization. *arXiv preprint arXiv:1607.06450*.
- Bommasani, R.; Hudson, D. A.; Adeli, E.; Altman, R.; Arora, S.; von Arx, S.; Bernstein, M. S.; Bohg, J.; Bosselut, A.; Brunskill, E.; et al. 2021. On the opportunities and risks of foundation models. *arXiv preprint arXiv:2108.07258*.
- Bouvier, J. 2006. Notes on convolutional neural networks.
- Chollet, F. 2017. Xception: Deep learning with depthwise separable convolutions. In *Proceedings of the IEEE conference on computer vision and pattern recognition*, 1251–1258.
- Chu, X.; Tian, Z.; Zhang, B.; Wang, X.; Wei, X.; Xia, H.; and Shen, C. 2021. Conditional positional encodings for vision transformers. *arXiv preprint arXiv:2102.10882*.
- Clancey, W. J. 1979. *Transfer of Rule-Based Expertise through a Tutorial Dialogue*. Ph.D. diss., Dept. of Computer Science, Stanford Univ., Stanford, Calif.
- Clancey, W. J. 1983. Communication, Simulation, and Intelligent Agents: Implications of Personal Intelligent Machines for Medical Education. In *Proceedings of the Eighth International Joint Conference on Artificial Intelligence (IJCAI-83)*, 556–560. Menlo Park, Calif: IJCAI Organization.
- Clancey, W. J. 1984. Classification Problem Solving. In *Proceedings of the Fourth National Conference on Artificial Intelligence*, 45–54. Menlo Park, Calif.: AAAI Press.
- Clancey, W. J. 2021. The Engineering of Qualitative Models. Forthcoming.
- Dai, J.; Qi, H.; Xiong, Y.; Li, Y.; Zhang, G.; Hu, H.; and Wei, Y. 2017. Deformable convolutional networks. In *Proceedings of the IEEE international conference on computer vision*, 764–773.
- Deng, J.; Dong, W.; Socher, R.; Li, L.-J.; Li, K.; and Fei-Fei, L. 2009. Imagenet: A large-scale hierarchical image database. In *2009 IEEE conference on computer vision and pattern recognition*, 248–255. Ieee.
- Dong, X.; Bao, J.; Chen, D.; Zhang, W.; Yu, N.; Yuan, L.; Chen, D.; and Guo, B. 2022. Cswin transformer: A general vision transformer backbone with cross-shaped windows. In *Proceedings of the IEEE/CVF Conference on Computer Vision and Pattern Recognition*, 12124–12134.
- Dosovitskiy, A.; Beyer, L.; Kolesnikov, A.; Weissenborn, D.; Zhai, X.; Unterthiner, T.; Dehghani, M.; Minderer, M.; Heigold, G.; Gelly, S.; et al. 2020. An image is worth 16x16 words: Transformers for image recognition at scale. *arXiv preprint arXiv:2010.11929*.
- Engelmore, R.; and Morgan, A., eds. 1986. *Blackboard Systems*. Reading, Mass.: Addison-Wesley.
- Fan, H.; Xiong, B.; Mangalam, K.; Li, Y.; Yan, Z.; Malik, J.; and Feichtenhofer, C. 2021. Multiscale vision transformers. In *Proceedings of the IEEE/CVF international conference on computer vision*, 6824–6835.
- Guo, M.-H.; Xu, T.-X.; Liu, J.-J.; Liu, Z.-N.; Jiang, P.-T.; Mu, T.-J.; Zhang, S.-H.; Martin, R. R.; Cheng, M.-M.; and Hu, S.-M. 2022. Attention mechanisms in computer vision: A survey. *Computational visual media*, 8(3): 331–368.
- Han, K.; Wang, Y.; Chen, H.; Chen, X.; Guo, J.; Liu, Z.; Tang, Y.; Xiao, A.; Xu, C.; Xu, Y.; et al. 2022. A survey on vision transformer. *IEEE transactions on pattern analysis and machine intelligence*, 45(1): 87–110.
- Hasling, D. W.; Clancey, W. J.; and Rennels, G. 1984. Strategic explanations for a diagnostic consultation system. *International Journal of Man-Machine Studies*, 20(1): 3–19.
- Hasling, D. W.; Clancey, W. J.; Rennels, G. R.; and Test, T. 1983. Strategic Explanations in Consultation—Duplicate. *The International Journal of Man-Machine Studies*, 20(1): 3–19.
- He, K.; Chen, X.; Xie, S.; Li, Y.; Dollár, P.; and Girshick, R. 2022. Masked autoencoders are scalable vision learners. In *Proceedings of the IEEE/CVF conference on computer vision and pattern recognition*, 16000–16009.
- He, K.; Zhang, X.; Ren, S.; and Sun, J. 2016. Deep residual learning for image recognition. In *Proceedings of the IEEE conference on computer vision and pattern recognition*, 770–778.
- Hendrycks, D.; and Gimpel, K. 2016. Gaussian error linear units (gelus). *arXiv preprint arXiv:1606.08415*.
- Hoffer, E.; Ben-Nun, T.; Hubara, I.; Giladi, N.; Hoefler, T.; and Soudry, D. 2020. Augment your batch: Improving generalization through instance repetition. In *Proceedings of the IEEE/CVF Conference on Computer Vision and Pattern Recognition*, 8129–8138.
- Iandola, F.; Moskewicz, M.; Karayev, S.; Girshick, R.; Darrell, T.; and Keutzer, K. 2014. Densenet: Implementing efficient convnet descriptor pyramids. *arXiv preprint arXiv:1404.1869*.
- Kirillov, A.; Mintun, E.; Ravi, N.; Mao, H.; Rolland, C.; Gustafson, L.; Xiao, T.; Whitehead, S.; Berg, A. C.; Lo, W.-Y.; et al. 2023. Segment anything. *arXiv preprint arXiv:2304.02643*.
- Krizhevsky, A.; Hinton, G.; et al. 2009. Learning multiple layers of features from tiny images.
- Krizhevsky, A.; Sutskever, I.; and Hinton, G. E. 2012. Imagenet classification with deep convolutional neural networks. *Advances in neural information processing systems*, 25.
- Li, Y.; Mao, H.; Girshick, R.; and He, K. 2022. Exploring plain vision transformer backbones for object detection. In *European Conference on Computer Vision*, 280–296. Springer.
- Lin, T.-Y.; Maire, M.; Belongie, S.; Hays, J.; Perona, P.; Ramanan, D.; Dollár, P.; and Zitnick, C. L. 2014. Microsoft coco: Common objects in context. In *Computer Vision—ECCV 2014: 13th European Conference, Zurich, Switzerland, September 6–12, 2014, Proceedings, Part V 13*, 740–755. Springer.

- Liu, Z.; Lin, Y.; Cao, Y.; Hu, H.; Wei, Y.; Zhang, Z.; Lin, S.; and Guo, B. 2021. Swin transformer: Hierarchical vision transformer using shifted windows. In *Proceedings of the IEEE/CVF international conference on computer vision*, 10012–10022.
- Loshchilov, I.; and Hutter, F. 2017. Decoupled weight decay regularization. *arXiv preprint arXiv:1711.05101*.
- Luo, W.; Li, Y.; Urtasun, R.; and Zemel, R. 2016a. Understanding the effective receptive field in deep convolutional neural networks. *Advances in neural information processing systems*, 29.
- Luo, W.; Li, Y.; Urtasun, R.; and Zemel, R. 2016b. Understanding the effective receptive field in deep convolutional neural networks. *Advances in neural information processing systems*, 29.
- NASA. 2015. Pluto: The 'Other' Red Planet. <https://www.nasa.gov/nh/pluto-the-other-red-planet>. Accessed: 2018-12-06.
- Paszke, A.; Gross, S.; Massa, F.; Lerer, A.; Bradbury, J.; Chanan, G.; Killeen, T.; Lin, Z.; Gimelshein, N.; Antiga, L.; et al. 2019. Pytorch: An imperative style, high-performance deep learning library. *Advances in neural information processing systems*, 32.
- Polyak, B. T.; and Juditsky, A. B. 1992. Acceleration of stochastic approximation by averaging. *SIAM journal on control and optimization*, 30(4): 838–855.
- Rice, J. 1986. Poligon: A System for Parallel Problem Solving. Technical Report KSL-86-19, Dept. of Computer Science, Stanford Univ.
- Robinson, A. L. 1980a. New Ways to Make Microcircuits Smaller. *Science*, 208(4447): 1019–1022.
- Robinson, A. L. 1980b. New Ways to Make Microcircuits Smaller—Duplicate Entry. *Science*, 208: 1019–1026.
- Rogozhnikov, A. 2022. Einops: Clear and Reliable Tensor Manipulations with Einstein-like Notation. In *International Conference on Learning Representations*.
- Sanders, J.; and Kandrot, E. 2010. *CUDA by example: an introduction to general-purpose GPU programming*. Addison-Wesley Professional.
- Simonyan, K.; and Zisserman, A. 2014. Very deep convolutional networks for large-scale image recognition. *arXiv preprint arXiv:1409.1556*.
- Szegedy, C.; Liu, W.; Jia, Y.; Sermanet, P.; Reed, S.; Anguelov, D.; Erhan, D.; Vanhoucke, V.; and Rabinovich, A. 2015. Going deeper with convolutions. In *Proceedings of the IEEE conference on computer vision and pattern recognition*, 1–9.
- Tan, M.; and Le, Q. 2019. Efficientnet: Rethinking model scaling for convolutional neural networks. In *International conference on machine learning*, 6105–6114. PMLR.
- Theodoridis, S.; and Koutroumbas, K. 2006. *Pattern recognition*. Elsevier.
- Tolstikhin, I. O.; Houlsby, N.; Kolesnikov, A.; Beyer, L.; Zhai, X.; Unterthiner, T.; Yung, J.; Steiner, A.; Keysers, D.; Uszkoreit, J.; et al. 2021. Mlp-mixer: An all-mlp architecture for vision. *Advances in neural information processing systems*, 34: 24261–24272.
- Touvron, H.; Cord, M.; Douze, M.; Massa, F.; Sablayrolles, A.; and Jégou, H. 2021. Training data-efficient image transformers & distillation through attention. In *International conference on machine learning*, 10347–10357. PMLR.
- Vaswani, A.; Shazeer, N.; Parmar, N.; Uszkoreit, J.; Jones, L.; Gomez, A. N.; Kaiser, L.; and Polosukhin, I. 2017a. Attention Is All You Need. *arXiv:1706.03762*.
- Vaswani, A.; Shazeer, N.; Parmar, N.; Uszkoreit, J.; Jones, L.; Gomez, A. N.; Kaiser, L.; and Polosukhin, I. 2017b. Attention is all you need. *Advances in neural information processing systems*, 30.
- Wang, J.; Sun, K.; Cheng, T.; Jiang, B.; Deng, C.; Zhao, Y.; Liu, D.; Mu, Y.; Tan, M.; Wang, X.; et al. 2020. Deep high-resolution representation learning for visual recognition. *IEEE transactions on pattern analysis and machine intelligence*, 43(10): 3349–3364.
- Wang, W.; Xie, E.; Li, X.; Fan, D.-P.; Song, K.; Liang, D.; Lu, T.; Luo, P.; and Shao, L. 2021. Pyramid vision transformer: A versatile backbone for dense prediction without convolutions. In *Proceedings of the IEEE/CVF international conference on computer vision*, 568–578.
- Weems, C. C.; Levitan, S. P.; Hanson, A. R.; Riseman, E. M.; Shu, D. B.; and Nash, J. G. 1989. The image understanding architecture. *International Journal of computer vision*, 2: 251–282.
- Werbos, P. J. 1994. *The roots of backpropagation: from ordered derivatives to neural networks and political forecasting*, volume 1. John Wiley & Sons.
- Wightman, R. 2019. PyTorch Image Models. <https://github.com/rwightman/pytorch-image-models>.
- Wu, H.; Xiao, B.; Codella, N.; Liu, M.; Dai, X.; Yuan, L.; and Zhang, L. 2021. Cvt: Introducing convolutions to vision transformers. In *Proceedings of the IEEE/CVF international conference on computer vision*, 22–31.
- Xie, Z.; Zhang, Z.; Cao, Y.; Lin, Y.; Bao, J.; Yao, Z.; Dai, Q.; and Hu, H. 2022. Simmim: A simple framework for masked image modeling. In *Proceedings of the IEEE/CVF Conference on Computer Vision and Pattern Recognition*, 9653–9663.
- Yu, F.; and Koltun, V. 2015. Multi-scale context aggregation by dilated convolutions. *arXiv preprint arXiv:1511.07122*.
- Zhou, B.; Zhao, H.; Puig, X.; Fidler, S.; Barriuso, A.; and Torralba, A. 2017. Scene parsing through ade20k dataset. In *Proceedings of the IEEE conference on computer vision and pattern recognition*, 633–641.

Appendix

MSA-Conv Implementation Details

In this paper, we propose the MSA-Conv, which involves extracting local regions of $K \times K$ from the input token map. And then applies self-attention to these local regions and extends the computation to the entire map through a sliding window mechanism, effectively combining global and local information (i.e as the model layers become deeper, TiC can obtain a global receptive field as ResNet (Chollet 2017)). During implementation, we initially explored using PyTorch’s Unfold function (Paszke et al. 2019) for extracting the sliding window-like values but found it computationally inefficient for large feature maps. To overcome this, we adopted C++ for CUDA programming (Sanders and Kandrot 2010) to efficiently implement MSA-Conv’s forward and backward propagation, significantly reducing computational consumption. Specifically, we implement our MSA-Conv in two parts: (1) \mathcal{O}_{QK} : use \mathbf{Q} and \mathbf{K} to compute \mathbf{Dot} , (2) \mathcal{O}_{DV} : use \mathbf{Dot} and \mathbf{V} to calculate the outputs, and the forward propagation is formulated as:

$$\begin{aligned} \mathcal{O}_{QK} &= \frac{\mathbf{Q} \times \mathbf{K}^T}{\sqrt{d^k}} \\ \mathbf{Dot} &= \text{softmax}(\mathcal{O}_{QK}) \\ \mathcal{O}_{DV} &= \mathbf{Dot} \times \mathbf{V} \end{aligned} \quad (3)$$

where d^k represents the length of the vector, \mathcal{O}_{QK} and \mathcal{O}_{DV} are based on CUDA programming, and softmax are directly called from pytorch interface (Paszke et al. 2019). For the specific symbolic derivation of the backward, since we have divided the implementation into two parts, \mathcal{O}_{QK} and \mathcal{O}_{DV} , we need to derive the gradient of \mathbf{Q} , \mathbf{K} , \mathbf{Dot} , and \mathbf{V} respectively, which is also divided into two parts. The formulation of the backward propagation is defined as:

$$\begin{aligned} \frac{\partial \mathcal{L}}{\partial \mathbf{Q}_{b,c,w,h}} &= \sum_{i=0}^{K-1} \sum_{j=0}^{K-1} \text{Unfold}(\mathbf{K})_{b,i,j,c,w,h} \\ \frac{\partial \mathcal{L}}{\partial \mathbf{K}_{b,c,h,w}} &= \sum_{i=0}^{K-1} \sum_{j=0}^{K-1} q_{b,c,i_1,j_1} \cdot \tilde{\mathbf{O}}_{k-1-a,k-1-b,i_1,j_1} \\ \frac{\partial \mathcal{L}}{\partial \mathbf{Dot}_{b,k^2,h,w}} &= \sum_{i=0}^{K-1} \sum_{j=0}^{K-1} v_{b,c,i_1,j_1} \cdot \tilde{\mathbf{O}}_{k-1-a,k-1-b,i_1,j_1} \\ \frac{\partial \mathcal{L}}{\partial \mathbf{V}_{b,c,w,h}} &= \sum_{i=0}^{K-1} \sum_{j=0}^{K-1} \text{Unfold}(\mathbf{Dot})_{b,i,j,c,w,h} \end{aligned} \quad (4)$$

where b, c, w, h represent the shape of \mathbf{Q} , b, k^2, w, h represent the shape of \mathbf{Dot} , $\tilde{\mathbf{O}}$ represents the gradient of the results obtained from the \mathcal{O}_{DV} , $i_1 = h - \frac{k-1}{2} + i$, $j_1 = w - \frac{k-1}{2} + j$, Unfold represents the PyTorch function (Paszke et al. 2019). Finally, we verify the reliability of our backward derivation by comparing the results obtained by the automated gradient derivation of PyTorch (Paszke et al. 2019) with those obtained by our own defined gradient

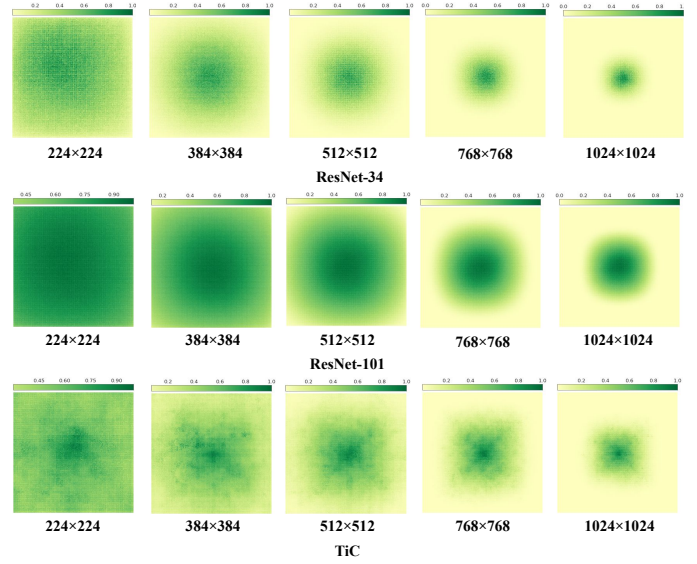


Figure 8: Illustration of effective receptive field of ResNet and TiC in various resolution images

derivation. The gradient value of the gradient formulation (Werbos 1994) is defined by:

$$\frac{\delta f}{\delta x} = \lim_{\Delta \rightarrow 0} \frac{f(x + \Delta) - f(x - \Delta)}{2\Delta} \quad (5)$$

where f represents the goal function (e.g. \mathcal{O}_{QK} , \mathcal{O}_{DV}), x represents the input, and $\Delta = 1e-7$.

Architecture Setup

In this work, we use TiC-B to complete our experiments, and the specific parameters of our TiC-B configuration are shown in Table. 4:

TiC-B	Inter Pooling	Kernel Size	Dilation Ratio	Depthwise Size	Dim Layer	Dim Head	Dim Depth
Stage1	2	3	4	7	128	4	2
Stage2	2	3	4	7	256	8	2
Stage3	1	3	4	5	512	16	18
Stage4	1	3	4	5	1024	32	2

Table 4: The architecture of TiC-B.

Benefiting from the flexibility of MSA-Conv, which can set different kernel sizes, the TiC architecture can be designed with many variants, and this paper is mainly based on TiC-B for subsequent experiments.

Modular MSA-Conv Exploratory Experiment

In this section, we further explored the application of modular Multi-Head Self-Attention Convolution in other Conv-Based architectures. As illustrated in Figure 8, the utilization of the sliding window mechanism manifests a parallel alteration in the effective receptive field for both our TiC and ResNet architectures as the image scale varies. This congruence in the receptive field behavior signifies a level of interrelation between our TiC model and Convolution-Based

Methods	Image size	Cifar-100
		Top-1 acc (%)
ViT-B	32 ²	54.31
TiC-B	32 ²	56.88
ResNet18	32 ²	75.61
ResNet18+MSA-Conv	32 ²	60.45
ResNet50	32 ²	77.39
ResNet50+MSA-Conv	32 ²	61.91

Table 5: Comparison of different backbones pretraining on Cifar-100 (Krizhevsky, Hinton et al. 2009)

architectures. Furthermore, we interfaced MSA-Conv based on pytorch to build a Conv-Like Layer and use it as a convolution layer added to mainstream Conv-Based architectures. Specifically, we added MSA-Conv Layer after the second convolutional layer of Bottleneck in ResNet-18, ResNet-50 (He et al. 2016), then tested it on Cifar-100 (Krizhevsky, Hinton et al. 2009), and compared the results with ResNet, TiC and ViT. The experimental results are shown in Table 5.

We can observe that for Transformer-Based architectures, due to the amount of data and image information of Cifar-100, it is difficult to train a network with such a large amount of parameters, so it shows low performance on Top-1 acc, e.g. ViT-B: 54.31, TiC-B: 56.88. For Conv-Based architectures, we exploratory add our MSA-Conv to each bottleneck of ResNet18, ResNet50, thus constructing a structure similar to Conv + Attention. It can be seen from the experimental results that thanks to the network structure of Conv-Based architectures, the results of our ResNet18+MSA-Conv, ResNet50+MSA-Conv have a certain performance improvement compared with ViT-B and TiC-B on Cifar-100. In addition, thanks to the mechanism of Conv, our ResNet18+MSA-Conv, ResNet50+MSA-Conv, like ResNet, can accept input of any resolutions without reprocessing the image or configuration.

In summation, we believe that future research should delve further into modular MSA-Conv and Conv-Based architectures, possibly influencing ViT-based models by synergizing Self-Attention and Convolution for improved outcomes. This has the potential to bolster the model’s performance and flexibility.